Journal of Power Sources 448 (2020) 227368

Contents lists available at ScienceDirect

Journal of Power Sources

journal homepage: www.elsevier.com/locate/jpowsour

A regenerative braking system for internal combustion engine vehicles using supercapacitors as energy storage elements - Part 1: System analysis and modelling

Emiliano Pipitone [a], Gianpaolo Vitale [b,*]

[a] Department of Engineering, University of Palermo, Italy
[b] ICAR, Institute for High Performance Computing and Networking, National Research Council of Italy, Italy

HIGHLIGHTS

- An electric KERS for internal combustion engine vehicles is proposed and studied .
- The KERS makes use of a supercapacitor bank as energy storage element. .
- A detailed mathematical model for the KERS performance evaluation is presented. .
- The efficiency of each KERS component is evaluated as function of time. .

GRAPHICAL ABSTRACT

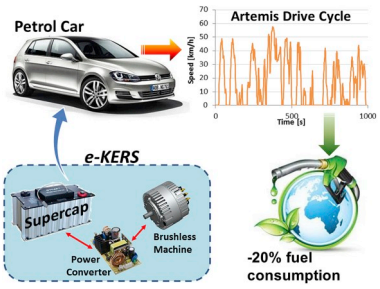

ARTICLE INFO

Keywords:
Kinetic energy recovery system
Supercapacitor
Ultracapacitor
Vehicle fuel economy
Regenerative braking
Urban driving cycle
Hybrid vehicle

ABSTRACT

In this two-part work, an electric kinetic energy recovery system (e-KERS) for internal combustion engine vehicle (ICEV) is presented, and its performance evaluated through numerical simulations. The KERS proposed is based on the use of a supercapacitor as energy storage, interfaced to a brushless machine through a properly designed power converter. In part 1, the system is described and analysed, and the mathematical model used for the simulations is presented. For each component of the KERS, the real efficiency, and the power or energy limitations are adequately considered. In part 2, the energetic and economic advantages attainable by the proposed KERS are evaluated using MATLAB Simulink, considering a widely diffused passenger car and two reference driving cycles (ECE-15 and Artemis Urban). Energy savings of the order of 20% were found, with a slight increase in vehicle weight (+2%) and with an overall commercial cost that would be compensated in 5 years thanks to the fuel economy improvement, to which corresponds an equal reduction of CO_2 emissions. The low complexity of the system, never proposed for ICEV, the moderate weight of its components, and their availability on the market, make the solution presented ready for the introduction in current vehicle production.

1. Introduction

The growing demand for sustainable mobility is driving researchers and vehicles manufacturers towards the exploration of low fuel consumption and environment-friendly solutions. The ever growing attention to road transport emission and urban pollution [1], the advances in

* Corresponding author.
E-mail address: gianpaolo.vitale@icar.cnr.it (G. Vitale).

https://doi.org/10.1016/j.jpowsour.2019.227368
Received 20 June 2019; Received in revised form 16 October 2019; Accepted 29 October 2019
Available online 14 November 2019
0378-7753/

the combustion and control of alternative and cost effective fuels [2,3], the optimal management of vehicles drive-lines [4,5] as well as the energy management techniques applied to electrified vehicles [6–9] are only few examples of the strong technological effort towards a sustainable and emission free mobility. Nevertheless, one of the heaviest lack in the management of traditional internal combustion engines vehicles (ICEV) is the huge amount of energy lost during braking phases. The kinetic energy of a vehicle, if recovered and not dissipated as heat by the traditional braking system, can be efficiently employed for successive vehicle acceleration phases or for general vehicle energy requirement, and could substantially contribute to lower the energy consumption of the vehicles and the pollution associated. Studies show that, in urban driving situations, conventional braking systems discard as heat to the atmosphere about one third to one half of the energy of the power plant [10].

Several regenerative braking systems (RBS) or kinetic energy recovery systems (KERS) have been proposed in literature, studied and optimized for different kind of vehicles (electric, hybrid or internal combustion engine vehicle), with different energy storage systems (mechanical, electrical, chemical, hydraulic), and suitable or not for retrofit application on current production vehicles.

Regenerative braking has been intensively studied and implemented on hybrid electric vehicles (HEV) and fuel cell hybrid electric vehicles (FCHEV): in these vehicles, the presence of powerful electric machines (generator and motor) interfaced to high capacity energy storage (e.g. batteries[1]) easily allows to convert and store vehicle kinetic energy into electric energy, which is then employed for vehicle propulsion [11]. As a matter of fact, both HEV [12–14] and FCHEV [15–18] usually implement electric KERS, exploiting the main storage system used for the traction in conjunction with supercapacitors, which allow a reduction of batteries intervention during vehicle regenerative braking or startup, thus enhancing batteries life cycle and maintaining their capacity performance.

Also, pure electric vehicles (EV) may easily benefit from regenerative braking if equipped with an appropriately sized generator, i.e., a generator capable of managing the braking power [19–21]. Many RBS for electric vehicles are based on the combined use of supercapacitors and batteries; even if their first applications were characterized by a relatively low amount of power, the optimal energy management of the two different storage systems and the availability on the market of new batteries and supercapacitors has been allowing to increase the rated power of the vehicles [9,13,22–26]. The voltage adaptation between the starter/generator and/or the battery is usually performed by suitable power converters able to guarantee a bidirectional flow of energy with high efficiency [21,27]. In any case, the use of supercapacitor as unique storage solution in electric vehicles remains limited since their energy density cannot compete with batteries. A RBS used in an electric truck employing only supercapacitors showed that it is possible to conceive this storage system for traction purposes as well avoiding batteries if a low driving range can be accepted [28]. A comparison between supercapacitors and flywheels as secondary energy storage system on a pure electric vehicle [29] put in evidence that the use of SC is by far much more convenient than the use of a flywheel to manage extreme startup and regenerative braking. Recently, supercapacitors have also been conceived in railway systems where it is appreciable the improvement of energy consumption efficiency and reducing peak power demand and costs of operation in railways substations [30,31].

Unlike electrified vehicles, internal combustion engine vehicles are not equipped with generator, electric motor and batteries of adequate power and capacity to allow the conversion of the vehicle kinetic energy into electric energy, as well as its storage and re-utilization for vehicle propulsion. For this reason, the kinetic energy recovery systems successfully tested for ICEV application are mainly based on mechanical and hydraulic energy storage devices. Spring and elastomers, for example, have been considered as storage elements of the KERS, relying on the (mechanical) energy storable by deforming an elastomer or a metallic spring [32]: the main advantage consists on the efficiency of the system since the conversion into electric energy is not required. Simulations revealed that a 15% potential fuel economy improvement can be achieved, but, besides a significant space to be fitted, the system also requires the use of a continuous variable transmission (CVT), thus adding complexity and significant weight to the vehicle.

Another pure mechanical system is represented by flywheel KERS, which stores the kinetic energy of the vehicle into rotational energy of a flywheel. As reported in literature [32,33] a flywheel-based KERS can recover up to 70% of vehicle kinetic energy and can reduce the fuel consumption of about 20%. Unfortunately, the energy recovered cannot be stored for a long time, due to mechanical and fluid dynamics friction on the flywheel. For this reason, vacuum chamber and magnetic bearings must be employed to obtain the best results. Moreover, to fully exploit its potential, this kind of KERS requires the use of a CVT and of lightweight composite flywheel: as an overall result, besides the added weight (65 kg for a 1800 kg vehicle), these high-technology components substantially increase the cost and complexity of the system. Average values for power and energy storage of high tech flywheel KERS are around 60 kW and 400 kJ, respectively [33].

Pneumatic and hydraulic KERS have also been studied for internal combustion engine vehicles: in these cases energy is stored by increasing the pressure of a fluid, which can be air (pneumatic type [34]) or a non-compressible fluid (hydraulic type [32]); the energy is then released back to the powertrain by decreasing the pressure of the fluid. Simulations showed that the pneumatic KERS with 300 kJ of energy storage may achieve a fuel efficiency improvement of about 20%, while a vehicle efficiency improvement of 35% is expected by hydraulic system with energy storage of 90 kJ. However, the additional space and weight of the added tanks and accumulators (considering a pneumatic type, a storage tank of 50 L is necessary for a 1-ton vehicle [34]) make this KERS more suitable for heavy vehicles, rather than for passenger cars. Moreover, the required modifications to the powertrain, which should be endowed of a CVT, make them unsuitable for retrofit.

The only kind of electric KERS currently studied and developed for internal combustion engine vehicles is represented by alternator-control KERS, which has been already introduced in the market by some car manufacturer (e.g., BMW Efficient Dynamics [35]): with this kind of systems, the alternator output is increased during braking phases, thus transferring part of the vehicle kinetic energy to the battery, whose energy is employed to supply electrical consumers of the vehicle, reducing the power absorbed by the alternator during vehicle positive traction phases. The advantage of this system relies on its immediate applicability to current ICEV production, but, being realized with components not dedicated or optimized for KERS application, the fuel economy improvement is limited, ranging from 1% to 5% [32].

In the present paper, the authors propose an electric KERS (e-KERS) for internal combustion engine vehicles composed of a supercapacitors bank (SC), used as electric energy storage system, a motor-generator unit (MGU) to convert vehicle kinetic energy into electric energy and vice versa, and a power converter (PC), whose task is to manage the power transfer between SC and MGU. The system was conceived to recover the vehicle kinetic energy during braking phases by charging the supercapacitor, whose stored energy is employed by the MGU for the successive vehicle acceleration. Even if, as already mentioned, SCs have been widely recognized in the last two decades as a valid storage system to face up with high peak power in hybrid vehicles [12–14], in electric vehicles [9,22,24,26,28] and in FCHEV [8,15–18], a wide literature research revealed that such an electric KERS has never been proposed or studied for ICEV application, above all employing a supercapacitor as single energy storage element. The use of a SC as single energy storage element has been proposed only when large spaces and weight were

[1] Although a battery is an energy converter, it is usually referred to as an energy storage, which is the same terminology adopted in this paper.

allowed, as in the case of electric city rail [36] or hybrid city bus [37], where energy saving of about 40% were obtained.

Differently from any other electric KERS proposed for ICEV, the system proposed in this paper allows to use the recovered energy for vehicle acceleration, rather than for electric users supply, thus substantially increasing the amount of recycled energy. Moreover, the low complexity of the system proposed, the reduced volume and weight of the components considered for KERS assembly and their immediate availability on the market, make the solution presented in this paper ready for the introduction in current vehicle production: this could substantially contribute to lower fuel consumption and the related pollutant emissions. Furthermore, differently from Formula 1 application,[2] where the sizing of the KERS aims to maximize propulsion power [38], the guidelines followed in the present work aim to optimize the overall vehicle cost without causing a marked weight increase, thus allowing the power to be optimally managed during braking and acceleration phases.

In this two-part study, the authors evaluate the plausible reduction of fuel consumption, and related CO_2 emissions, that could be achieved by the implementation of the electric KERS proposed in traditional passenger cars endowed of the internal combustion engine (ICE), with the aim to improve their sustainability and environmental compatibility. The analysis performed in this first part aims to develop the mathematical tool for the simulation of the regenerative braking phase and the acceleration phase of the vehicle endowed with the KERS, while the evaluation of the energetic, environmental and economic benefits will be shown in the second part.

It is also worth to highlight that the system proposed may contribute to the hybridization process of ICEV, already started with the development of the so-called starter-generators system [39], whose growth in power, control complexity and launching ability could further promote the use of supercapacitors as energy storage elements for KERS application.

2. System description

The kinetic energy recovery system proposed in this work is schematically represented in Fig. 1 together with the vehicle drivetrain: the supercapacitor (SC), which is the energy storage part of the system, is electrically interfaced, through an expressly designed power converter (PC), to the motor-generator unit (MGU), which is mechanically connected to the drive shaft via a fixed gear ratio. As it is clear, the whole system is conceived to be bidirectional, allowing the mechanical power to be converted into electrical power during vehicle braking phases, storing the recovered energy into the SC, and vice versa, using the stored energy to supply the electric motor to produce mechanical power during vehicle acceleration.

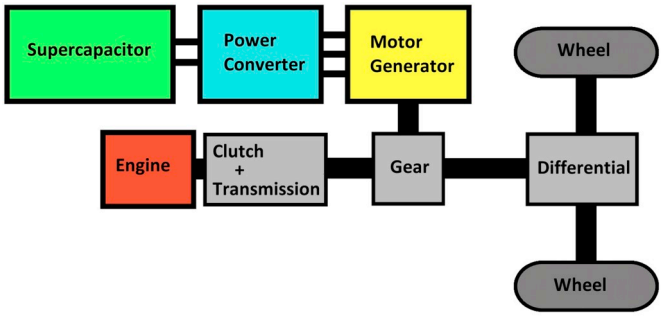

Fig. 1. Drivetrain layout of the vehicle with KERS.

The most interesting element of the KERS considered in this work is represented by the supercapacitor unit. Supercapacitors (often called ultracapacitors) are available on the market with capacitance values up to 3000 F and rated voltage up to 125 V, obtained by means of suitable series-parallel combinations of single SC units [40]. Supercapacitors have recently drawn more attention than batteries because of their faster response, implying a low discharge time (1–10 s for SCs against 10–60 min for lithium-ion batteries) and enhanced cyclic stability (greater than 30,000 h for SCs, and only 500 h for batteries). A supercapacitor may hence be considered as a current pulse system to meet high current and specific power (10,000 W kg^{-1}) requirements for time interval within 1 min, as required in a drive system to fulfil the power demand for starting and recovering braking energy [9,11,20,25,26,28,29]. Supercapacitors can withstand half-million of cycles because of their storage mechanisms, which do not involve a reversible chemical reaction, and can operate at temperatures between −40 and 100 °C [41] whereas batteries can be operated only between −20 and 60 °C [42,43]. A crucial role in these advantages is played by materials. In particular, to achieve a good capacitance rating, a good electrode-electrolyte match is required [44]. New technologies and materials are described in Ref. [45], where the most attractive materials for electrodes (such as carbon-based materials, metal oxides, and conducting polymers) are presented, together with flexible solid state and quasi solid state supercapacitors [46], which employ metallic ions to enhance the energy density; finally waste materials are also proposed as highly cheap option to obtain supercapacitor electrodes, although some improvements are still necessary. Increasing attention is also being paid to flexible supercapacitors, above all as energy storage for wearable electrical devices [47], alone or in conjunction with solar cells [48], also supported by the use of carbon nanotube fibers [49].

As regards the MGU, the authors focused on brushless motors due to their prerogative of high efficiency, fast dynamic response, higher power density and longer lifetime with respect to common brushed motor; more in details, three-phase permanent magnet synchronous motors (PMSM) were selected for their prerogative of delivering high torque with low ripple; as it is known, this kind of motor requires a proper controller for the transformation of the DC power into three phases AC power. In the system proposed, the function of the power converter is to manage the power flow between the supercapacitor and the MGU: to this purpose it comprises both a DC/DC converter to fit the SC voltage to the MGU voltage (and vice versa), and an inverter for the control of the MGU through proper sinusoidal current waveforms. It must also be pointed out that, in this work, the brushless motor is assumed to be current-controlled, i.e., the torque delivered (or received) is controlled by controlling the phase-currents, as described in Ref. [50]. In the case here considered, the power converter, whose block diagram is reported in Fig. 2, is a buck/boost converter that can be operated in both step-up and step-down configuration, thus adapting the voltage of the SC to the voltage of the MGU [51]; its interleaved topology offers several advantages compared to a traditional single inductor topology: the current

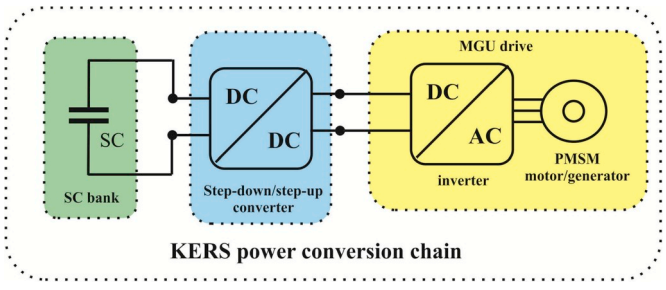

Fig. 2. Scheme of the KERS proposed: as shown the power converter comprises both a DC/DC converter and a DC/AC inverter.

[2] In this case the energy storage has been realized by the use of lithium-ion battery pack.

can be shared among the inductors, thus allowing to reduce conduction losses; when small currents are concerned, a single inductor can be used, and the ripple on the current can be reduced by a phase displacement of the pulse width modulation signals, allowing a lower switching frequency to be adopted with advantage in terms of the minimization of switching losses.

These conversion topologies have been recently studied to achieve high conversion efficiency assessing a high power density and a reduced cost per kW; a discussion on the optimization of the power converter is beyond of the scope of this paper, but further information can be found in Refs. [51–53].

The efficiency curve of such power converter [51] is reported in Fig. 3 as function of output and input percentage power (due to the high efficiency level, the two curves are almost overlapping): as it can be seen, for a power factor in the order of 5%, the efficiency reaches 0.90, while for power factor exceeding 10% of maximum, the efficiency remains at its best value, i.e., 0.93.

The KERS proposed in this work is supposed to operate only during the transient vehicle phases, participating to vehicle acceleration in conjunction with the internal combustion engine, or to vehicle braking in conjunction with the mechanical braking system (e.g., a disc brake system or a drum brake system). More in detail, during a braking phase, the MGU acts as a generator and contributes to reducing the vehicle speed transferring part of the vehicle kinetic energy to the supercapacitor. During regenerative braking, hence, the power flows from the vehicle wheels to the MGU which charges the supercapacitor: in this case, the power converter fits the voltage of the MGU drive to the voltage of the SC and regulates the electric current supplied to the SC according to the power received by the MGU.

During an acceleration phase, instead, the MGU acts as a motor and contributes to increasing vehicle speed, thus reducing the power demand to the internal combustion engine and, as a consequence, its fuel consumption and the related CO_2 emissions. During an acceleration phase, hence, the MGU, supplied by the SC through the power converter, transmits the power to the drive shaft and therefore to the wheels: in this case, hence, the power converter adapts the SC voltage to the MGU voltage and controls the power transfer from the supercapacitor regulating the electric current supplied to the MGU.

Considering the structure of the proposed KERS (see Fig. 1), the power flux involving each element is schematically reported in Fig. 4 both for acceleration and for braking phase; this diagram helps to identify the magnitude of the power managed by each component of the KERS.

3. Vehicle dynamics

In general, the elementary equation which takes into account all the forces acting on the longitudinal dynamics of a vehicle is:

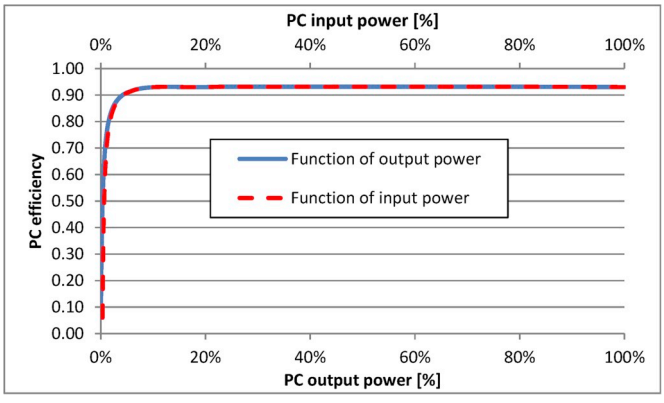

Fig. 3. Power converter efficiency as function of both percentage output and input power.

$$F_{trac}(t) - F_{br}(t) - \left[F_{aer}(t) + F_{roll}(t) + F_{grav}(t) + F_{dist}(t)\right] = m_v \cdot \frac{d\,v(t)}{dt} = m_v \cdot a(t) \tag{1}$$

where m_v represents the reference mass of the vehicle (which should also comprise the equivalent mass of the rotating parts), $v(t)$ and $a(t)$ are the vehicle speed and acceleration (functions of time t), F_{trac} is the traction force acting on the vehicle as result of the overall motive power, F_{br} is the braking force acting on the vehicle as result of the braking system, F_{aer} is the drag force due to the impact with the air, F_{roll} is the rolling resistance force on the wheels, F_{grav} is the force of gravity acting in the case of a slope and F_{dist} takes into account any other disturbance force of motion, as it could be for example the wind.

The sum of the forces within square brackets constitutes the *road load* F_{road}, which is the resistance to movement and must be overcome by the vehicle to move forward.

$$F_{road}(t) = F_{aer}(t) + F_{roll}(t) + F_{grav}(t) + F_{dist}(t) \tag{2}$$

Hence equation (1) becomes:

$$F_{trac}(t) - F_{br}(t) - F_{road}(t) = m_v \cdot a(t) \tag{3}$$

It is worth to underline that both the resistance to movement F_{road} and the braking force F_{br} always act in the opposite direction of the vehicle speed, thus producing a braking effect; as can be observed in equation (3), in this work these forces have been considered positive, leaving their braking role to the negative sign; on the contrary, the traction force F_{trac} is considered positive when acting in the same direction of vehicle speed. To the purpose of this work, the contributions due to F_{grav} and F_{dist} forces were neglected, since the vehicles were considered to operate in a horizontal plane and without any disturbing forces (as therefore assumed for the execution of standard driving cycles). The aerodynamic resistance F_{aer} can be calculated as:

$$F_{aer}(v) = \frac{1}{2}\delta_a \cdot A_f \cdot c_x(v) \cdot v^2 \tag{4}$$

where δ_a represents the air density ($1.225\,\mathrm{kg\,m^{-3}}$ in standard conditions), A_f is the frontal area of the vehicle and c_x is the drag coefficient, which takes into account the air resistance on the vehicle's profile and may vary with vehicle speed. The rolling resistance F_{roll} can be evaluated as:

$$F_{roll}(v) = c_r(v,p) \cdot m_v \cdot g \tag{5}$$

being g the gravitational acceleration and c_r the rolling resistance coefficient, which, besides a marked dependence on the vehicle speed v, should also vary with the tires pressure p. For convenience, however, in this work both the drag coefficient c_x and the rolling resistance coefficient c_r were considered constant.

As a result, multiplying the forces of equation (1) for the vehicle speed $v(t)$, the power balance is obtained:

$$P_{trac}(t) - P_{br}(t) = F_{road}(t) \cdot v(t) + m_v \cdot a(t) \cdot v(t) = P_{road}(t) + P_I(t) \tag{6}$$

where P_{road} ($=F_{road} \cdot v$) is the *road load power*, that is the power necessary to counterbalance the resistance to movement, while P_I ($=m_v \cdot a \cdot v$) is the *inertial power* which instead accounts for the power required by inertia force. As already pointed out, both braking power P_{br} and road load power P_{road} have been considered positive, being their braking function left to the negative sign with respect to traction power.

Equation (6) comprises both traction and braking forces, which in practical situations are not simultaneously present. In a real application, instead, one of the following motion conditions is realized: acceleration, constant speed, braking, coasting.

An acceleration process is characterized by $a(t) > 0$ and obviously $P_{br}=0$, hence

$$P_{trac}(t) = m_v \cdot a(t) \cdot v(t) + P_{road}(t) = P_I(t) + P_{road}(t) \tag{7}$$

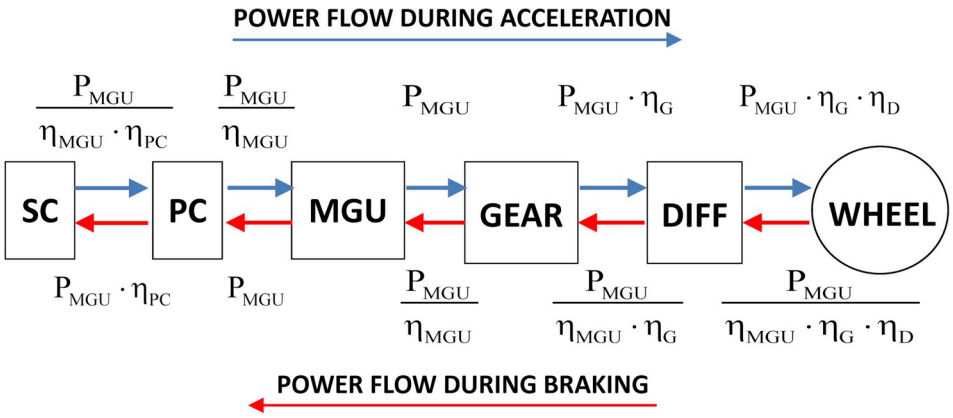

Fig. 4. Schematic representation of the KERS power fluxes in both acceleration and braking phase.

to perform the acceleration $a(t) > 0$, the vehicle requires the sum of the road load power P_{road} (>0) and the inertial power P_I (positive because $a(t) > 0$). In other words, due to the braking effect of the resistance to the movement, the energy required to accelerate the vehicle is higher than the variation of the vehicle kinetic energy. In the KERS here proposed, the function of the MGU, during an acceleration phase, is to contribute to the inertial power P_I, exploiting the energy stored in the supercapacitor, thus reducing the power demand to the thermal engine. The road load power P_{road} is instead considered entirely balanced by the thermal engine, which also has to supply the remaining part of the inertial power. It is evident that, if the MGU completely fulfils the inertial power P_I, the internal combustion engine has to provide only the road load power.

When moving with constant speed, $a(t)=0$ and $P_{br}=0$, hence

$$P_{trac}(t) = P_{road}(t) \tag{8}$$

the inertia force is null and the vehicle requires only the power necessary to counterbalance the resistance to movement. In this condition, the KERS proposed by the authors does not operate.

When coasting, the vehicle proceeds without traction or braking forces ($P_{br}=0$, $P_{trac}=0$), and hence, as shown by equation (3), reduces its speed with a negative acceleration ($a(t) < 0$) as a result of the resistance to movement:

$$m_v \cdot a(t) = -F_{road}(t) \tag{9}$$

or, which is the same,

$$P_I(t) = m_v \cdot a(t) \cdot v(t) = -P_{road}(t) \tag{10}$$

According to the approach followed in this paper, also this condition does not imply any KERS operation.

In a braking phase, instead, the negative vehicle acceleration is the effect of braking action, hence $P_{br}>0$ (and obviously $P_{trac}=0$); equation (6) thus gives:

$$P_{br}(t) = -m_v \cdot a(t) \cdot v(t) - P_{road}(t) = -P_I(t) - P_{road}(t) \tag{11}$$

which means that, to produce the required negative acceleration $a(t)$, due to the braking effect of the road load, the power that the braking system (which may include the action of the KERS) must absorb is lower than the absolute value of the inertial power. This means that the inertial power cannot be entirely recovered during regenerative braking, but only the fraction $P_{br}(t)$. In other words, due to the braking effect of the road load, the vehicle kinetic energy cannot be entirely recovered. The function of the MGU during such a braking phase is, hence, to convert and transfer (as much as possible) part of the braking power $P_{br}(t)$ to the supercapacitor, whose stored energy will be employed for successive vehicle accelerations.

4. Mathematical model

The evaluation of the energetic performances obtainable by the system proposed was carried out through numerical simulation performed by MATLAB Simulink. In the following sections, a detailed description of the equations employed in the numerical simulations is given; for a better understanding, the reader should refer to the power fluxes reported in Fig. 4. As already clarified, the KERS proposed in this paper is supposed to operate only during transient phases, reducing the power demand to the thermal engine during vehicle accelerations, and recovering part of the vehicle kinetic energy during the braking phases. It is worth to point out that the calculation always proceeds from the wheel (where the required acceleration or braking power is known) to the supercapacitor: as a result, in the simulation regarding vehicle acceleration, for each element of the KERS, the output power was determined first; in the simulation regarding vehicle braking, instead, the input power of each KERS component was evaluated first.

4.1. Acceleration phases

Focusing on the acceleration phases (i.e. $a(t) > 0$), the required vehicle traction power (see equation (7)) can be written as:

$$P_{trac}(t) = P_I(t) + P_{road}(t) = \left[P_{MGU}(t) \cdot \eta_G + P_{eng}(t) \cdot \eta_T\right] \cdot \eta_D \tag{12}$$

being the net contribution of the MGU reduced by the efficiency η_G of the gear adopted (as represented in Fig. 1) between the brushless motor and the drive shaft, P_{eng} the power demand to the internal combustion engine, η_T and η_D the efficiency of the main transmission and of the final differential gear respectively. It is worth to remember that the vehicle acceleration condition is $a(t) > 0$ ($\Rightarrow P_I(t) > 0$) and differs from $P_{trac}(t) > 0$, since, due to the road load power $P_{road}(t)$, the traction power $P_{trac}(t)$ is positive also when the vehicle proceeds with constant speed ($a(t) = 0$).

As regards the brushless motor, a model was adopted to evaluate the input power $P_{MGU,in}(t)$ of the motor as a function of the output power $P_{MGU}(t)$. The power balance of the brushless motor can be represented as:

$$P_{MGU}(t) = T_{MGU}(t) \cdot \omega(t) = P_{MGU,in}(t) - L_{MGU}(t) - I \cdot \alpha(t) \cdot \omega(t) \tag{13}$$

where the output power $P_{MGU}(t)$ is the product between the motor rotation speed $\omega(t)$ and the torque $T_{MGU}(t)$ delivered, $L_{MGU}(t)$ represents the sum of the power losses in the MGU, and the last term represents the inertial power absorbed by the brushless motor (whose rotational inertia is I) subjected to the angular acceleration $\alpha(t)$. On the basis of [54,55] the power losses in the MGU were subdivided into:

1) resistive and power interrupter losses, $L_R(t)$

2) mechanical friction losses, $L_F(t)$
3) windage losses, $L_W(t)$

The first kind of losses mainly depend on the square value of the MGU phase current, and, in turn, on the square value of the current on the DC side of the MGU controller $i_{MGU}(t)$. Indicating with R the proportionality constant, the resistive losses can be expressed as:

$$L_R(t) = R \cdot {i_{MGU}}^2(t) \tag{14}$$

As regards the second kind of losses, according to the usual hypothesis of constant friction torque = T_F, a proportionality with the rotor angular velocity $\omega(t)$ can be assumed, i.e.:

$$L_F(t) = T_F \cdot \omega\ (t) \tag{15}$$

The third kind of losses, as is generally done, were considered proportional to the cube of the rotor angular velocity by means of the parameter k. Summing up, the power losses in the MGU were modelled as:

$$L_{MGU}(t) = L_R(t) + L_F(t) + L_W(t) = R \cdot i_{MGU}^2(t) + T_F \cdot \omega\ (t) + k \cdot \omega^3(t) \tag{16}$$

The losses parameters R, T_F, and k of the MGU can be obtained using statistical regression of the experimental data provided by the motor manufacturer. As an example, Fig. 5 shows the agreement between the measured efficiency and the efficiency computed by the model for the brushless motor Motenergy M1115 [56].

Once calibrated, the motor model allows to determine the necessary DC input power to the MGU (i.e. $P_{MGU,in}(t)$), which must be provided by the power converter as the product of the supply voltage V_{MGU} for the current $i_{MGU}(t)$:

$$P_{PC}(t) = P_{MGU,in}(t) = V_{MGU} \cdot i_{MGU}(t) \tag{17}$$

The power balance of the brushless motor of equation (13) hence becomes:

$$\begin{aligned} &V_{MGU} \cdot i_{MGU}(t) - T_{MGU}(t) \cdot \omega\ (t) - R \cdot {i_{MGU}}^2(t) - T_F \cdot \omega\ (t) - k \cdot \omega^3(t) \\ &\quad - I \cdot \alpha\ (t) \cdot \omega\ (t) \\ &\quad = 0 \end{aligned} \tag{18}$$

Equation (18) allows determining the input current to the MGU controller $i_{MGU}(t)$, once the torque to deliver $T_{MGU}(t)$ is known. Three constraints must be however taken into consideration: the first regards the torque delivered by the motor, which is limited by the stall torque $T_{MGU,stall}$, which is a characteristic of the brushless machine. The second constraint regards, instead, the input current to the MGU controller, which cannot exceeds the maximum allowed value $i_{MGU,max}$, that is another important characteristic of the brushless machine. This further limits the torque that the brushless motor can deliver to the value $T_{MGU,CL}(t)$, which can be obtained by equation (18) once the maximum current $i_{MGU,max}$ is considered, i.e.:

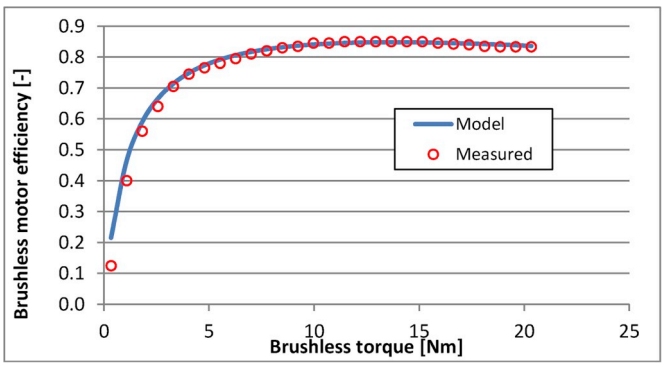

Fig. 5. Comparison between measured and simulated brushless motor efficiency (based on Motenergy ME1115, 69 V_{DC}, 3000 rpm [56]).

$$T_{MGU,CL}(t) = \frac{V_{MGU} \cdot i_{MGU,\max}(t)}{\omega\ (t)} - \frac{R \cdot {i_{MGU,\max}}^2(t)}{\omega\ (t)} - T_F - k \cdot \omega^2(t) - I \cdot \alpha\ (t) \tag{19}$$

It is worth noting that the current limited torque $T_{MGU,CL}(t)$ depends on the motor rotation speed $\omega(t)$.

Besides the two constraints already mentioned, in the system proposed the power produced by the brushless motor can be further limited by the instantaneous power availability at the supercapacitor $P_{SC,max}(t)$:

$$P_{SC,max}(t) = V_{SC}(t) \cdot i_{PC,max} \tag{20}$$

this power availability depends on the instantaneous working voltage $V_{SC}(t)$ of the supercapacitor, which continuously varies during KERS operation together with the amount of energy stored (and is evaluated through equation (35)), and on the maximum current allowed in the power converter $i_{PC,max}$, which, as will be shown in the paper Part 2, is determined in the KERS sizing procedure to meet its power requirement.

As also shown by Fig. 4, the limited output power availability at the supercapacitor may limit the input power to the MGU, whose working current may hence be restricted to:

$$i_{MGU,SL}(t) = \frac{P_{SC,max}(t) \cdot \eta_{PC}(t)}{V_{MGU}} = \frac{V_{SC}(t) \cdot i_{PC,max} \cdot \eta_{PC}(t)}{V_{MGU}} \tag{21}$$

being $\eta_{PC}(t)$ the power converter efficiency, whose value, as shown further on, can be evaluated through equation (31). As a result, the motor output torque is further limited to the value $T_{MGU,SL}(t)$ obtained by equation (18) once the supercapacitor limited current $i_{MGU,SL}(t)$ of equation (21) is considered, i.e.:

$$T_{MGU,SL}(t) = \frac{V_{MGU} \cdot i_{MGU,SL}(t)}{\omega\ (t)} - \frac{R \cdot {i_{MGU,SL}}^2(t)}{\omega\ (t)} - T_F - k \cdot \omega^2(t) - I \cdot \alpha\ (t) \tag{22}$$

For each rotation speed $\omega(t)$, hence, the maximum torque $T_{MGU,max}(t)$ that the brushless motor can deliver is:

$$T_{MGU,\max}(t) = \min(T_{MGU,stall}; T_{MGU,CL}(t); T_{MGU,SL}(t)) \tag{23}$$

and the consequent maximum motive power that the brushless motor can deliver is:

$$P_{MGU,\max}(t) = T_{MGU,\max}(t) \cdot \omega\ (t) \tag{24}$$

As clarified by the layout reported in Fig. 1, the motor rotation speed $\omega(t)$ depends on the vehicle speed $v(t)$ through the vehicle wheel radius R_W, the brushless gear ratio τ_G and the final gear ratio τ_D:

$$\omega\ (t) = \frac{v(t)}{R_W} \cdot \tau_G \cdot \tau_D \tag{25}$$

Analogously, the motor acceleration $\alpha(t)$ can be evaluated on the basis of the vehicle acceleration $a(t)$:

$$\alpha(t) = \frac{d\omega\ (t)}{dt} = \frac{a(t)}{R_W} \cdot \tau_G \cdot \tau_D \tag{26}$$

Both wheel radius R_W and differential final gear ratio τ_D depend on the vehicle while the brushless gear ratio τ_G was fixed considering to reach the maximum motor rotation speed at the vehicle speed of 60 km h^{-1} (i.e., the maximum value within urban driving cycles): it is worth to point out that, according to the system proposed, brushless motor and drive shaft must be disengaged when vehicle speed exceeds 60 km h^{-1}.

As already clarified, in the present paper the motor contribution was restricted to the inertial power $P_I(t)$ necessary for vehicle acceleration; as a consequence, in the simulation performed, the power produced by the MGU was evaluated as:

$$P_{MGU}(t) = \min\left(P_{MGU,\max}(t);\ \frac{P_I(t)}{\eta_G \cdot \eta_D}\right) \tag{27}$$

where the gear efficiency η_G was assumed 0.97 while the efficiency of the differential η_D was assumed 0.93.

Once determined the power produced by the MGU, the power demand to the internal combustion engine P_{eng} can be deduced from equation (12) as the necessary complement to the total required traction power:

$$P_{eng}(t) = \frac{P_{trac}(t)}{\eta_D \cdot \eta_T} - \frac{P_{MGU}(t)}{\eta_T} \cdot \eta_G = \frac{P_I(t) + P_{road}(t)}{\eta_D \cdot \eta_T} - \frac{P_{MGU}(t)}{\eta_T} \cdot \eta_G \quad (28)$$

In the system proposed, during an acceleration phase, the MGU is supplied by the power converter, whose output power $P_{PC}(t)$, as also shown in Fig. 4, constitutes the input power $P_{MGU,in}(t)$ to the MGU and can be determined by equations (17) and (18). The power converter, in turn, is supplied by the supercapacitor, whose output power (as shown in Fig. 4) is hence:

$$P_{SC}(t) = \frac{P_{PC}(t)}{\eta_{PC}(t)} \quad (29)$$

being $\eta_{PC}(t)$ the power converter efficiency, evaluated on the basis of the normalized output power ($=P_{PC}(t)/P_{PC,max}$) through equation (30). It is worth to note that the limit of the maximum available power at the supercapacitor $P_{SC,max}(t)$ is already respected through equation (27).

As regards the power converter efficiency $\eta_{PC}(t)$, an analysis performed by means of Curve Expert on the data plotted in Fig. 3 allowed to determine its expression as a function of the normalized output power $x_{PC}(t)=P_{PC}(t)/P_{PC,max}$:

$$\eta_{PC}(t) = 0.930 - 1.009 \cdot exp(-26.16 \cdot x_{PC}(t)^{0.6128}) \quad (30)$$

or as function of the normalized input power $x_{PC,in}(t)=P_{PC,in}(t)/P_{PC,in,max}$:

$$\eta_{PC}(t) = 0.930 - 280.7 \cdot exp(-15.82 \cdot x_{PC,in}(t)^{0.1766}) \quad (31)$$

The energy content of the supercapacitor during the (emptying) acceleration process is hence evaluated through the integration of the power delivered by the supercapacitor, taking into account its efficiency:

$$E_{SC}(t) = \int_{E_i} dE_{SC} = \int_{E_i} -\frac{P_{SC}(t)}{\eta_{SC}(t)} \, dt \quad (32)$$

where E_i denotes the initial energy content of the SC. The efficiency of the supercapacitor was evaluated by means of its equivalent series resistance (ESR):

$$\eta_{SC}(t) = 1 - \frac{i_{SC}(t) \cdot ESR}{V_{SC}(t)} \quad (33)$$

where $V_{SC}(t)$ and $i_{SC}(t)$ represent the supercapacitor instantaneous working voltage and current. Given the relation between the energy stored in the supercapacitor $E_{SC}(t)$ and its working voltage:

$$E_{SC}(t) = \frac{1}{2} \cdot C \cdot V_{SC}^2(t) \quad (34)$$

the supercapacitor working voltage is evaluated as:

$$V_{SC}(t) = \sqrt{\frac{2 \cdot E_{SC}(t)}{C}} \quad (35)$$

being C the nominal capacitance of the supercapacitor.

The supercapacitor current can be hence evaluated on the basis of the power demand $P_{SC}(t)$ calculated in equation (29):

$$i_{SC}(t) = \frac{P_{SC}(t)}{V_{SC}(t)} \quad (36)$$

The supercapacitor voltage $V_{SC}(t)$ also allows to determine its instantaneous maximum available power $P_{SC,max}(t)$:

$$P_{SC,max}(t) = V_{SC}(t) \cdot i_{PC,max} \quad (37)$$

which represents the maximum power that during an acceleration phase can be delivered by the supercapacitor to the converter, and puts a limit to the supercapacitor rate of discharge (equations (32)) and to the power delivered by the brushless motor (equations (21)).

To account for the necessary minimum working voltage of the supercapacitor $V_{SC,min}$ (assumed to correspond to 40% of the rated storable energy), the integral of equation (32) is limited in the lower values, i.e., a minimum is imposed to the energy stored in the supercapacitor:

$$E_{SC,\min} = 0.4 \cdot E_{SC,\max} = \frac{1}{2} \cdot C \cdot V_{SC,\min}^2 \quad (38)$$

Once reached this minimum energy content in the SC, the system is considered unable to produce power for vehicle acceleration, and the MGU output is considered null, thus making all the necessary traction power $P_{trac}(t)$ entirely provided by the thermal engine:

$$P_{MGU}(t) = 0 \quad \text{if} \quad \begin{cases} a(t) > 0 \\ \text{AND} \\ E_{SC}(t) = E_{SC,\min} \end{cases} \quad (39)$$

4.2. Braking phases

Focusing now on vehicle braking phases, the power $P_{br}(t) > 0$ that must be absorbed for vehicle deceleration ($a(t) < 0$) is:

$$P_{br}(t) = -m_v \cdot a(t) \cdot v(t) - P_{road}(t) = -P_I(t) - P_{road}(t) \quad (40)$$

Unlike the acceleration case, the authors supposed that, in a braking phase, the KERS contribution is not restricted, to convert as much as possible of the braking power. However, also in this case, several constraints limit the power that can be recovered by the brushless machine, now acting as a generator, or by the supercapacitor. For the analysis of the brushless generator performances, a model was adopted to evaluate the power received and transferred, taking into account the same losses considered when acting as a motor, hence:

$$V_{MGU} \cdot i_{MGU}(t) = T_{MGU}(t) \cdot \omega(t) - i_{MGU}^2(t) \cdot R - T_F \cdot \omega(t) - k \cdot \omega^3(t) - I \cdot \alpha(t) \cdot \omega(t) \quad (41)$$

As it is clear, in a braking case, the input is the mechanical power $\omega(t) \cdot T_{MGU}(t)$ received through the drive shaft; after reductions due to resistive and power interrupter losses, to friction losses and windage losses, the remaining power is converted into DC electrical power $V_{MGU} \cdot i_{MGU}(t)$ by the inverter. It is worth noting that, in a braking phase, the brushless angular acceleration $\alpha(t)$ is negative, and hence the rotor inertial power constitutes a positive power input to the brushless generator. Given hence the mechanical input power, equation (41) allows to determine the current $i_{MGU}(t)$ and hence the related power transmitted by the brushless generator to the power converter.

Once again, several limitations must be adequately taken into account for the calculation of the power received and converted by the KERS: first of all, the maximum torque that the brushless generator can receive cannot exceeds the stall torque $T_{MGU,stall}$. The second limitation is represented by the maximum current $i_{MGU,max}$ allowed on the DC side of the MGU controller, which further restricts the torque that can be transformed by the brushless generator to the value $T_{MGU,CL}(t)$, evaluated through equation (41) with the use of the maximum allowed current, i.e.:

$$T_{MGU,CL}(t) = \frac{V_{MGU} \cdot i_{MGU,\max}(t)}{\omega(t)} + \frac{R \cdot i_{MGU,\max}^2(t)}{\omega(t)} + T_F + k \cdot \omega^2(t) + I \cdot \alpha(t) \quad (42)$$

As also pointed out in the acceleration case, the current limited torque $T_{MGU,CL}(t)$ depends on the motor rotation speed $\omega(t)$.

The third limitation to consider is related to the maximum power that the supercapacitor can receive $P_{SC,max}(t)$ (see equation (54)), which may limit the power transfer between MGU and power converter, and hence, the input torque to the generator; considering that, in the braking case, the current limit imposed by the supercapacitor is:

$$i_{MGU,SL}(t) = \frac{P_{SC,max}(t)}{V_{MGU} \cdot \eta_{PC}(t)} = \frac{V_{SC}(t) \cdot i_{PC,max}}{V_{MGU} \cdot \eta_{PC}(t)} \tag{43}$$

it follows that the torque received by the brushless generator is limited to the value $T_{MGU,SL}(t)$ obtained by equation (41) when the current $i_{MGU,SL}(t)$ is considered:

$$T_{MGU,SL}(t) = \frac{V_{MGU} \cdot i_{MGU,SL}(t)}{\omega\ (t)} + \frac{R \cdot {i_{MGU,SL}}^2(t)}{\omega\ (t)} + T_F + k \cdot \omega^2(t) + I \cdot \alpha\ (t) \tag{44}$$

In equation (43) the power converter efficiency $\eta_{PC}(t)$ is determined through equation (30) on the basis of the normalized output power $x_{PC}=P_{SC,max}(t)/P_{PC,max}$.

As a result, for each rotation speed $\omega(t)$, the maximum torque $T_{MGU,max}(t)$ that the brushless generator can receive during a braking phase is:

$$T_{MGU,\max}(t) = \min(T_{MGU,stall}; T_{MGU,CL}(t); T_{MGU,SL}(t)) \tag{45}$$

and hence, the maximum power that the brushless machine can receive during a braking phase is:

$$P_{MGU,in,\max}(t) = T_{MGU,\max}(t) \cdot \omega\ (t) \tag{46}$$

Taking into consideration the efficiency η_G of the brushless gear, the input power to the brushless generator $P_{MGU,in}(t)$ can be computed once the braking power $P_{br}(t)$ is known:

$$P_{MGU,in}(t) = \min(P_{MGU,in,\max}(t)\ ;\ P_{br}(t) \cdot \eta_G \cdot \eta_D\ ) \tag{47}$$

Once determined the power received by the MGU, the input power $P_{PC,in}(t)$ to the converter is computed through equation (41):

$$P_{PC,\text{in}}(t) = V_{MGU} \cdot i_{MGU}(t) = P_{MGU,in}(t) - {i_{MGU}}^2(t) \cdot R - T_F \cdot \omega\ (t) - k \cdot \omega^3(t) - I \cdot \alpha\ (t) \cdot \omega\ (t) \tag{48}$$

The power input to the supercapacitor is hence evaluated as:

$$P_{SC,in}(t) = P_{PC,\text{in}}(t) \cdot \eta_{PC}(t) = V_{MGU} \cdot i_{MGU}(t) \cdot \eta_{PC}(t) \tag{49}$$

where the efficiency $\eta_{PC}(t)$ of the power converter is computed by means of equation (31) on the basis of its normalized input power $x_{PC,in}=P_{PC,in}(t)/P_{PC,in,max}$.

The energy content of the supercapacitor during a (filling) braking phase is then determined integrating its effective input power, i.e.:

$$E_{SC}(t) = \int_{E_i} dE_{SC} = \int_{E_i} P_{SC,in}(t) \cdot \eta_{SC}(t)\ \ dt \tag{50}$$

where the SC efficiency is again evaluated as:

$$\eta_{SC}(t) = 1 - \frac{i_{SC}(t) \cdot ESR}{V_{SC}(t)} \tag{51}$$

being $V_{SC}(t)$ the SC working voltage calculated by means of the energy content $E_{SC}(t)$ and of the capacitance C of the supercapacitor:

$$V_{SC}(t) = \sqrt{\frac{2 \cdot E_{SC}(t)}{C}} \tag{52}$$

while the current $i_{SC}(t)$ is evaluated on the basis of the power input to the supercapacitor (equation (49)):

$$i_{SC}(t) = \frac{P_{SC,in}(t)}{V_{SC}(t)} \tag{53}$$

The supercapacitor voltage $V_{SC}(t)$ also allows to determine its instantaneous maximum input power $P_{SC,\ max}(t)$:

$$P_{SC,max}(t) = V_{SC}(t) \cdot i_{PC,max} \tag{54}$$

which, as shown in equation (47), limits the power that can be transferred during a braking phase, and hence the supercapacitor rate of charge (equations (50)).

As obvious, the integration in equation (50) was limited to the maximum energy storable in the supercapacitor, which is:

$$E_{SC,\max} = \frac{1}{2} \cdot C \cdot V_{SC,\max}^2 \tag{55}$$

Once reached this upper limit, the KERS is considered unable to receive further power, the input power to the MGU is considered null, thus making all the necessary braking power $P_{br}(t)$ entirely provided by the mechanical braking system of the vehicle:

$$P_{MGU,in}(t) = 0 \quad \text{if} \quad \begin{cases} P_{br}(t) > 0 \\ \text{AND} \\ E_{SC}(t) = E_{SC,\max} \end{cases} \tag{56}$$

5. Discussion

The mathematical model presented in this paper is intended to simulate the regenerative braking phases and the acceleration phases of an internal combustion engine vehicle endowed of the proposed KERS. With the aim to fairly evaluate the performance of the system proposed and to obtain useful and reliable results from simulations, the authors carefully took into account the losses which could impair the efficiency of both energy recovery and energy re-utilization. However, a possible source of error of the mathematical model may derive from the not considered parasitic resistances of cables and contacts, which, in the real system, will be necessarily present to connect the KERS components. The authors decided to left out these resistances because their magnitude greatly depends on the real system layout (e.g., on the distance between the supercapacitor, power converter, and brushless machine) and, as a general rule, should remain negligible with respect to the main losses already considered.

Reproducibility, which is a fundamental aspect of scientific and technological research, was also considered by the authors: when dealing with numerical simulations, reproducibility allows a different team to reproduce the same simulation experiment based on the detailed specifications of its scenario and of the model employed [57]. The author focused hence on both model reproducibility and results reproducibility, as defined in Ref. [58]. As regards the model reproducibility, meaning to provide sufficient details about procedures and data so that the same evaluation can be exactly repeated, the model was given in terms of simple power balance equations, involving either the whole vehicle or some particular element of the KERS. The equations of the model can be numerically integrated, or implemented by a suitable software (Simulink was employed by the authors, as reported in the second part of this work), to describe the behavior of the studied system and the power flows between the KERS components. Several parameters take part in the definition of the model equations, with different origin:

1) some parameters are derived from the scientific literature, as, for example, the tires rolling resistance coefficient, the final drive efficiency, the fixed gear ratio efficiency, etc.
2) other parameters are derived from vehicle specifications (as example the vehicle mass and frontal surface area, wheel radius, drag coefficient, etc.) or by the manufacturer of the KERS component (e.g. the maximum voltage levels and maximum allowed currents of supercapacitor and brushless machine, the MGU peak torque, the rated capacitance and ESR of the supercapacitor, the power converter efficiency, etc.)
3) other parameters instead are not directly provided and must be obtained by means of statistical regression performed on experimental

data provided by the manufacturer, as the losses parameters of the MGU, which, as already shown in Fig. 5, were obtained minimizing the mean square error between the experimental efficiency values obtained by the manufacturer and the efficiency values obtained by the losses model of equation (16).

As regards the results reproducibility, meaning to obtain the same results from an independent study with same procedures of the original study, the scenario (intended as the exogenous stimuli applied to the system [57]) must be adequately defined. For the application considered in this study, the scenario is represented by the vehicle speed and acceleration as a function of time, besides vehicle specifications and KERS features. As reported in the second part of this work, the authors adopted standard driving cycles (ECE-15 and Artemis Urban were considered) as standard scenario not only to guarantee the reproducibility of simulations and results, but also to allow the experimental validation of the findings. Moreover, with the aim to limit the reproducibility error, all the necessary parameters have been considered using at least three significant digits.

6. Conclusions

In this first part of a two-papers work, the authors propose an electric KERS for internal combustion engine vehicle. The system was conceived to recover the vehicle kinetic energy during braking phases, to be reused in successive vehicle acceleration phases, so as to reduce the power demand to the internal combustion engine, and, as a consequence, the related fuel consumption and pollutant emissions. An accurate description of the system proposed is given in this first paper, together with a detailed mathematical model realized by the authors with the aim to evaluate the probable energetics and economics performances of the KERS by numerical simulations. For each component of the KERS, the model evaluates its real efficiency during operation, taking into account the limitations introduced in terms of both storable energy or transferrable power. The energetic benefits introduced by the implementation of the proposed KERS on a passenger car are evaluated in the second part of this work by means numerical simulation performed with Matlab Simulink.

Declaration of competing interest

The authors declare that they have no known competing financial interests or personal relationships that could have appeared to influence the work reported in this paper.

References

[1] P. Iodice, A. Senatore, Experimental-analytical investigation to estimate an emission inventory from road transport sector, in: IAENG Transactions on Engineering Sciences - Special Issue of the International MultiConference of Engineers and Computer Scientists, IMECS 2013 and World Congress on Engineering, WCE 2013, 2014, pp. 141–149.

[2] P. Iodice, A. Senatore, G. Langella, A. Amoresano, Advantages of ethanol–gasoline blends as fuel substitute for last generation Si engines, Environ. Prog. Sustain. Energy 36 (4) (2017) 1173–1179, https://doi.org/10.1002/ep.12545.

[3] E. Pipitone, G. Genchi, Experimental determination of liquefied petroleum gas-gasoline mixtures knock resistance, J. Eng. Gas Turbines Power 136 (12) (2014), https://doi.org/10.1115/1.4027831, 121502.

[4] M. Cammalleri, D. Rotella, Functional design of power-split CVTs: an uncoupled hierarchical optimized model, Mech. Mach. Theory 116 (2017) 294–309.

[5] D. Rotella, M. Cammalleri, Direct analysis of power-split CVTs: a unified method, Mech. Mach. Theory 121 (2018) 116–127.

[6] Y. Zhou, A. Ravey, M.C. Péra, A survey on driving prediction techniques for predictive energy management of plug-in hybrid electric vehicles, J. Power Sources 412 (2019) 480–495, https://doi.org/10.1016/j.jpowsour.2018.11.085.

[7] W. Zhou, L. Yang, Y. Cai, T. Ying, Dynamic programming for new energy vehicles based on their work modes Part II: fuel cell electric vehicles, J. Power Sources 407 (2018) 92–104, https://doi.org/10.1016/j.jpowsour.2018.10.048.

[8] P. Thounthong, S. Raël, B. Davat, Control strategy of fuel cell/supercapacitors hybrid power sources for electric vehicle, J. Power Sources 158 (1) (2006) 806–814, https://doi.org/10.1016/j.jpowsour.2005.09.014.

[9] E. Faggioli, P. Rena, V. Danel, X. Andrieu, R. Mallant, H. Kahlen, Supercapacitors for the energy management of electric vehicles, J. Power Sources 84 (2) (1999) 261–269, https://doi.org/10.1016/S0378-7753(99)00326-2.

[10] G. Sovran, D. Blaser, Quantifying the Potential Impacts of Regenerative Braking on a Vehicle's Tractive-Fuel Consumption for the U.S., European, and Japanese Driving Schedules, 2006. SAE Technical Paper 2006-01-0664.

[11] Q. Xu, F. Wang, X. Zhang, S. Cui, Research on the Efficiency Optimization Control of the Regenerative Braking System of Hybrid Electrical Vehicle Based on Electrical Variable Transmission, IEEE, 2019. Early Access Article, Digital Object Identifier 10.1109/ACCESS.2017.

[12] L. Solero, A. Lidozzi, V. Serrao, L. Martellucci, E. Rossi, Ultracapacitors for fuel saving in small size hybrid vehicles, J. Power Sources 196 (1) (2011) 587–595, https://doi.org/10.1016/j.jpowsour.2009.07.041.

[13] A. Burke, M. Miller, The power capability of ultracapacitors and lithium batteries for electric and hybrid vehicle applications, J. Power Sources 196 (1) (2011) 514–522, https://doi.org/10.1016/j.jpowsour.2010.06.092.

[14] L. Rambaldi, E. Bocci, F. Orecchini, Preliminary experimental evaluation of a four wheel motors, batteries plus ultracapacitors and series hybrid powertrain, Appl. Energy 88 (2) (2011) 442–448, https://doi.org/10.1016/j.apenergy.2010.08.008.

[15] H. Li, A. Ravey, A. N'Diaye, A. Djerdir, A novel equivalent consumption minimization strategy for hybrid electric vehicle powered by fuel cell, battery and supercapacitor, J. Power Sources 395 (2018) 262–270, https://doi.org/10.1016/j.jpowsour.2018.05.078.

[16] M.G. Carignano, R. Costa-Castelló, V. Roda, N.M. Nigro, S. Junco, D. Feroldi, Energy management strategy for fuel cell-supercapacitor hybrid vehicles based on prediction of energy demand, J. Power Sources 360 (2017) 419–433, https://doi.org/10.1016/j.jpowsour.2017.06.016.

[17] P. Thounthong, S. Rael, B. Davat, Energy management of fuel cell/battery/supercapacitor hybrid power source for vehicle applications, J. Power Sources 193 (1) (2009) 376–385, https://doi.org/10.1016/j.jpowsour.2008.12.120.

[18] D. Feroldi, M. Carignano, Sizing for fuel cell/supercapacitor hybrid vehicles based on stochastic driving cycles, Appl. Energy 183 (2016) 645–658, https://doi.org/10.1016/j.apenergy.2016.09.008.

[19] E. Chemali, M. Preindl, P. Malysz, A. Emadi, Electrochemical and electrostatic energy storage and management systems for electric drive vehicles: state-of-the-art review and future trends, IEEE .J. Emerg.Sel. Top.Power Electron. 4 (3) (2016) 1117–1134, https://doi.org/10.1109/JESTPE.2016.2566583.

[20] K. Itani, A. De Bernardinis, Z. Khatir, A. Jammal, M. Oueidat, Regenerative braking modeling, control, and simulation of a hybrid energy storage system for an electric vehicle in extreme conditions, IEEE.Trans.Transp.Electrification 2 (4) (2016) 465–479, https://doi.org/10.1109/TTE.2016.2608763.

[21] F. Akar, Y. Tavlasoglu, E. Ugur, B. Vural, I. Aksoy, A bidirectional nonisolated multi-input DC–DC converter for hybrid energy storage systems in electric vehicles, IEEE Trans. Veh. Technol. 65 (10) (2016) 7944–7955, https://doi.org/10.1109/TVT.2015.2500683.

[22] L. Kouchachvili, W. Yaïci, E. Entchev, Hybrid battery/supercapacitor energy storage system for the electric vehicles, J. Power Sources 374 (2018) 237–248, https://doi.org/10.1016/j.jpowsour.2017.11.040.

[23] Ziyou Song, Heath Hofmann, Jianqiu Li, Jun Hou, Xuebing Han, Minggao Ouyang, Energy management strategies comparison for electric vehicles with hybrid energy storage system, Appl. Energy 134 (2014) (2014) 321–331, https://doi.org/10.1016/j.apenergy.2014.08.035, 0306–2619.

[24] K.M. So, Y.S. Wong, G.S. Hong, W.F. Lu, An Improved Energy Management Strategy for a Battery/Ultracapacitor Hybrid Energy Storage System in Electric Vehicles, IEEE Transportation Electrification Conference and Expo (ITEC), Dearborn, MI, 2016, pp. 1–6, https://doi.org/10.1109/ITEC.2016.7520186.

[25] W. Zhao, G. Wu, C. Wang, L. Yu, Y. Li, Energy transfer and utilization efficiency of regenerative braking with hybrid energy storage system, J. Power Sources 427 (2019) 174–183.

[26] H. Peng, J. Wang, W. Shen, D. Shi, Y. Huang, Controllable regenerative braking process for hybrid battery–ultracapacitor electric drive systems, IET Power Electron. 11 (15) (2018) 2507–2514.

[27] J. Kloetzl, D. Gerling, An interleaved buck-boost-converter combined with a supercapacitor-storage for the stabilization of automotive power nets, in: 2011 IEEE Vehicle Power and Propulsion Conference, 2011, pp. 1–6, https://doi.org/10.1109/VPPC.2011.6042982. Chicago, IL.

[28] Z. Zou, J. Cao, B. Cao, W. Chen, Evaluation strategy of regenerative braking energy for supercapacitor vehicle, ISA (Instrum. Soc. Am.) Trans. 55 (2015) 234–240, https://doi.org/10.1016/j.isatra.2014.09.011.

[29] K. Itani, A. De Bernardinis, Z. Khatir, A. Jammal, Comparative analysis of two hybrid energy storage systems used in a two front wheel driven electric vehicle during extreme start-up and regenerative braking operations, Energy Convers. Manag. 144 (2017) 69–87.

[30] G. Cui, L. Luo, C. Liang, S. Hu, Y. Li, Y. Cao, B. Xie, J. Xu, Z. Zhang, Y. Liu, T. Wang, Supercapacitor Integrated Railway Static Power Conditioner for Regenerative Braking Energy Recycling and Power Quality Improvement of High-Speed Railway System. Early Access Article, IEEE, 2019.

[31] M. Khodaparastan, A.A. Mohamed, W. Brandauer, Recuperation of regenerative braking energy in electric rail transit systems, IEEE Trans. Intell. Transp. Syst. 20 (2016) 2831–2884, https://doi.org/10.1109/TITS.2018.2886809.

[32] A. Gabriel-Buenaventura, B. Azzopardi, Energy recovery systems for retrofitting in internal combustion engine vehicles: a review of techniques, Renew. Sustain. Energy Rev. 41 (2015) 955–964, https://doi.org/10.1016/j.rser.2014.08.083.

[33] M. Thomas, D. Nishanth, Flywheel based kinetic energy recovery systems (KERS) integrated in vehicles, Int. J. Eng. Sci. Technol. 5 (09) (2013) 1694–1699, 0975-5462.

[34] Z. Dimitrova, F. Maréchal, Gasoline hybrid pneumatic engine for efficient vehicle powertrain hybridization, Appl. Energy 151 (2015) 168–177, https://doi.org/10.1016/j.apenergy.2015.03.057.
[35] http://www.bmw.com.af/com/en/insights/technology/efficientdynamics/phase_1/measures_brake_energy_regeneration.html. (Accessed February 2019).
[36] Jisheng Hu, Yukun Zhao, Xiaojing Liu, in: The Design of Regeneration Braking System in Light Rail Vehicle Using Energy-Storage Ultra-capacitor, 2008 IEEE Vehicle Power and Propulsion Conference, 2008, pp. 1–5, https://doi.org/10.1109/VPPC.2008.4677708. Harbin.
[37] M. Ouyang, W. Zhang, E. Wang, F. Yang, J. Li, Z. Li, P. Yu, X. Ye, Performance analysis of a novel coaxial power-split hybrid powertrain using a CNG engine and supercapacitors, Appl. Energy 157 (2015) 595–606, https://doi.org/10.1016/j.apenergy.2014.12.086.
[38] K. Upendra, A. Grauers, Analysis of 2014 Formula One Hybrid Powertrain, Chalmers University of Technology, Department of Signals and Systems, 2015. http://emobilitycentre.se/en/category/fordonsanalys/.
[39] B. Lequesne, Automotive electrification: the nonhybrid story, IEEE.Trans.Transp. Electrification 1 (1) (2015) 40–53, https://doi.org/10.1109/TTE.2015.2426573.
[40] G. Vitale, Supercapacitor modelling by Lagrange's equations, in: International Conference on Modern Electrical Power Engineering, (ICMEPE-2016), las Palmas de Gran Canaria 6 - 8 of July, 2016.
[41] M. Al Sakka, H. Gualous, J. Van Mierlo, H. Culcu, Thermal modeling and heat management of supercapacitor modules for vehicle applications, J. Power Sources 194 (2) (2009) 581–587, https://doi.org/10.1016/j.jpowsour.2009.06.038.
[42] K. Sharma, A. Arora, S.K. Tripathi, Review of supercapacitors: materials and devices, J. Energy Storage 21 (2019) 801–825.
[43] J. Libich, J. Máca, J. Vondrák, O. Čech, M. Sedlaříková, Supercapacitors: properties and applications, J. Energy Storage 17 (2018) 224–227.
[44] A. González, E. Goikolea, J.A. Barrena, R. Mysyk, Review on supercapacitors: technologies and materials, Renew. Sustain. Energy Rev. 58 (2016) 1189–1206.
[45] W. Raza, F. Ali, N. Raza, Y. Luo, K.-H. Kim, J. Yang, S. Kumar, A. Mehmood, E. E. Kwon, Recent advancements in supercapacitor technology, Nano Energy 52 (2018) 441–473, https://doi.org/10.1016/j.nanoen.2018.08.013.
[46] Y. Du, G. Li, M. Chen, X. Yang, L. Ye, X. Liu, L. Zhao, Hollow nickel-cobalt-manganese hydroxide polyhedra via MOF templates for high-performance quasi-solid-state supercapacitor, Chem. Eng. J. 378 (2019) 122210, https://doi.org/10.1016/j.cej.2019.122210.
[47] A. Pedico, A. Lamberti, A. Gigot, M. Fontana, F. Bella, P. Rivolo, M. Cocuzza, C. F. Pirri, High-performing and stable wearable supercapacitor exploiting rGO aerogel decorated with copper and molybdenum sulfides on carbon fibers, ACS Appl. Energy Mater. 1 (9) (2018) 4440–4447, https://doi.org/10.1021/acsaem.8b00904.
[48] A. Scalia, F. Bella, A. Lamberti, C. Gerbaldi, E. Tresso, Innovative multipolymer electrolyte membrane designed by oxygen inhibited UV-crosslinking enables solid-state in plane integration of energy conversion and storage devices, Energy 166 (2019) 789–795, https://doi.org/10.1016/j.energy.2018.10.162.
[49] N. Liu, Z. Pan, X. Ding, J. Yang, G. Xu, L. Li, Q. Wang, M. Liu, Y. Zhang, In-situ growth of vertically aligned nickel cobalt sulfide nanowires on carbon nanotube fibers for high capacitance all-solid-state asymmetric fiber-supercapacitors, J Energy.Chem. 41 (2020) 209–215, https://doi.org/10.1016/j.jechem.2019.05.008.
[50] J.W. Dixon, I.A. Leal, Current control strategy for brushless dc motors based on a common DC signal, IEEE Trans. Power Electron. 17 (2) (2002) 232–240, https://doi.org/10.1109/63.988834.
[51] G. Vitale, E. Pipitone, A six legs buck-boost interleaved converter for KERS application, submitted for publication to Renewable Energy & Power Quality Journal (RE&PQJ), ISSN: 2172-038X, currently available for consultation on, http://emilianopipitone.altervista.org/publication_list.htm, 2019.
[52] G. Vitale, Energy saving by power electronics: towards a new concept of renewable source, Invited paper - plenary Session, in: International Conference on Renewable Energies and Power Quality (ICREPQ'16) Madrid (Spain), 4th to 6th May, 2016.
[53] C. Gammeter, F. Krismer, J.W. Kolar, Comprehensive conceptualization, design, and experimental verification of a weight-optimized all-sic 2 kV/700 V DAB for an airborne wind turbine, IEEE .J. Emerg.Sel. Top.Power Electron. 4 (2) (2016) 638–656, https://doi.org/10.1109/JESTPE.2015.2459378.
[54] P. Andrada, M. Torrent, J.I. Perat, B. Blanqué, Power losses in outside-spin brushless D.C. Motors, Renewable Energy & Power Quality Journal 1 (2004), https://doi.org/10.24084/repqj02.320, 2.
[55] Kuria James, Pyung Hwang, Modeling power losses in electric vehicle BLDC motor, J. Energy Technol. Policy.ISSN 1 (4) (2011) 2224–3232.
[56] http://www.motenergy.com/me1115motor.html. (Accessed February 2019).
[57] Olivier Dalle, On Reproducibility and Traceability of Simulations, WSC - Winter Simulation Conference - 2012, Berlin, Germany, 2012, p. 244, hal-00782834.
[58] H.E. Plesser, Reproducibility vs. Replicability: a brief history of a confused terminology, Front. Neuroinf. 11 (2018) 76, https://doi.org/10.3389/fninf.2017.00076.

8. Symbols and abbreviations

a, a(t): vehicle acceleration, as function of time t
A_f: frontal area of the vehicle
C: capacitance
CNG: compressed natural gas
CVT: continuous variable transmission
c_r: rolling resistance coefficient
c_x: drag coefficient of the vehicle
E_{SC}: energy stored in the supercapacitor
$E_{SC,max}$: maximum storable energy in the supercapacitor
$E_{SC,min}$: minimum allowed energy content of the supercapacitor
ECE-15: European urban driving cycle
ESR: equivalent series resistance of the supercapacitor
EUDC: European extra urban driving cycle
F_{aer}: vehicle aerodynamic resistance
F_{br}: braking force acting on the vehicle
F_{dist}: external disturbance force acting on the vehicle
F_{grav}: force of gravity acting on the vehicle in the case of a slope
F_{road}: road load (vehicle resistance to the movement)
F_{roll}: vehicle rolling resistance
F_{trac}: traction force acting on the vehicle
I: MGU rotor inertia
i_{MGU}: current on the DC side of the MGU controller
$i_{MGU,\ max}$: maximum allowed current on the DC side of the MGU controller
$i_{MGU,\ SL}$: MGU current limit imposed by the maximum power output of the supercapacitor
$i_{PC,max}$: maximum allowed current in the power converter
i_{SC}: current in the supercapacitor
ICE: internal combustion engine
ICEV: internal combustion engine vehicle
k: windage losses constant of the MGU
KERS: kinetic energy recovery system
L_F: mechanical friction losses of the MGU
L_{MGU}: MGU power losses
L_R: resistive and power interrupter losses of the MGU
L_W: windage losses of the MGU
m_v: vehicle mass
MGU: motor-generator unit
$n_{MGU,\ max}$: maximum rotation speed of the MGU
NEDC: new European driving cycle
p: tires pressure
P_{br}: braking power
p_E: loss of energy Boolean variable
P_{eng}: power output from the internal combustion engine
P_I: inertial power
p_L: loss of power Boolean variable
P_{MGU}: power output from the MGU
$P_{MGU,max}$: maximum power output from the MGU
$P_{MGU,in}$: power input to the MGU
$P_{MGU,in,max}$: maximum power input to the MGU
P_{PC}: power output from the power converter
$P_{PC,max}$: maximum power output from the power converter
$P_{PC,in}$: power input to the power converter
$P_{PC,in,max}$: maximum power input to the power converter
P_{road}: road load power
P_{SC}: power output from the supercapacitor
$P_{SC,in}$: power input to the supercapacitor
$P_{SC,max}$: maximum power output from the supercapacitor
P_{trac}: traction power acting on the vehicle
PC: power converter
PMSM: permanent magnet synchronous motor
R: the resistive losses constant of the MGU
RMS: root mean square value
R_W: vehicle wheel radius
SC: supercapacitor
UDC: urban driving cycle
t: time
T_F: constant friction torque of the MGU
T_{MGU}: torque delivered by the MGU
$T_{MGU,max}$: maximum torque that the MGU can deliver (as motor) or receive a(as generator)
$T_{MGU,\ CL}$: MGU torque limit imposed by the maximum allowed current $i_{MGU,max}$
$T_{MGU,\ SL}$: MGU torque limit imposed by the maximum power output of the supercapacitor
$T_{MGU,\ stall}$: peak stall torque of the MGU
v, v(t): vehicle speed, as function of time t
V_{MGU}: voltage on the DC side of the MGU controller
$V_{MGU,\ max}$: maximum allowed voltage on the DC side of the MGU controller
V_{SC}: instantaneous working voltage of the supercapacitor
$V_{SC,\ max}$: maximum allowed voltage of the supercapacitor
WLTC: worldwide harmonized light vehicles test cycles
x_{PC}: normalized output power from the power converter
$x_{PC,in}$: normalized input power to the power converter
α(t): MGU angular acceleration (function of time)
δ_a: air density
η_D: efficiency of the final differential gear
η_G: efficiency of the gear between MGU and drive shaft
η_{MGU}: efficiency of the MGU
η_{PC}: efficiency of the power converter
η_{PC}^*: power converter efficiency at its maximum output power
η_{SC}: efficiency of supercapacitor
η_T: efficiency of the vehicle main transmission
τ_D: differential gear ratio
τ_G: MGU gear ratio
ω(t): MGU rotational speed (function of time)